

# Aggregation in carbon dots

Yi Ru<sup>1</sup>, Geoffrey I. N. Waterhouse<sup>1</sup>, and Lu Siyu<sup>2</sup>

<sup>1</sup>Affiliation not available

<sup>2</sup>Zhengzhou University

October 18, 2022

## Abstract

Carbon dots (CDs) possess outstanding luminescence properties, leading to their use in a wide range of applications including optical displays, anti-counterfeiting systems, bioimaging and sensors. Presently, there is much debate about the classification of CDs, as well as their formation process, structure and fluorescence mechanisms. Aggregation plays an important role in both the formation of CDs and their fluorescence (e.g. aggregation-induced emission), yet is seldom studied in detail. This review aims fill this knowledge gap, by firstly exploring how aggregation leads to the formation of different types of CDs (e.g. graphene quantum dots, carbon quantum dots, and carbonized polymer dots), followed by a detailed examination of the effect of aggregation-induced morphology on the luminescence properties and application of CDs. Finally, opportunities and challenges for the application of CDs in various applications are discussed, with the need for better mechanistic understanding of aggregation-induced luminescence being an imperative.

Aggregation in carbon dots

Yi Ru, Geoffrey I. N. Waterhouse, Siyu Lu\*

Dr. Yi Ru, Prof. Siyu Lu

Green Catalysis Center, and College of Chemistry, Zhengzhou University, Zhengzhou 450000, China. E-mail: sylvu2013@zzu.edu.cn

Prof. Geoffrey I. N. Waterhouse School of Chemical Sciences, The University of Auckland, Auckland 1142, New Zealand.

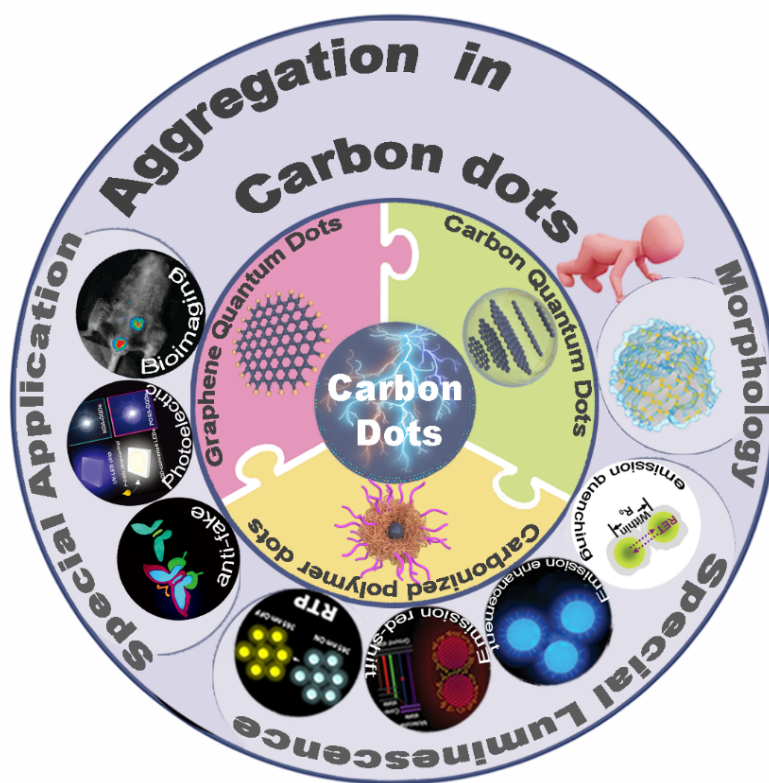
Keywords: carbon dots, aggregation, special morphology, special luminescence, special application

Carbon dots (CDs) possess outstanding luminescence properties, making them widely used in optical displays, anti-counterfeiting systems, bioimaging and sensors. Presently, there is much debate about the classification of CDs, as well as their formation process, structure and fluorescence mechanisms. Aggregation plays an important role in the formation and fluorescence (e.g. aggregation-induced emission) of CDs, yet is seldom studied in detail. This review aims fill this knowledge gap, by firstly exploring how aggregation leads to the formation of different types of CDs (e.g. graphene quantum dots, carbon quantum dots, and carbonized polymer dots), followed by a detailed examination of the effect of aggregation-induced morphology on the luminescence properties and application of CDs. Finally, opportunities and challenges for the application of CDs in various applications are discussed, with the need for better mechanistic understanding of aggregation-induced luminescence being an imperative.

## Introduction

The development of fluorescent nanomaterials has driven innovation in many fields, including photoelectric devices, bioimaging, biomedicine, sensing, and many other areas.<sup>[1-5]</sup> Unlike conventional aggregation-induced

quenching in molecules, many fluorescent nanomaterials show negligible emission at low concentrations but emit intensely in the aggregated state. Aggregation-induced emission was first proposed by Tang et al. [6] in 2001. Aggregation-induced emission is now being exploited in chemical sensing, environmental monitoring, biological imaging, optoelectronic devices, medical diagnosis and treatment, amongst other applications.[7-9] This has motivated research aimed at better understanding of the luminescence of aggregates,[10] with innovative mechanisms proposed to account for different emission phenomena, including clusterization-triggered emission, through-space interactions, and so forth.[11, 12]



Scheme 1. Different types of CDs and role of aggregation in their formation, morphology, luminescence properties and applications.

As a novel kind of fluorescent nanomaterial, carbon dots (CDs) have enormous attention since they were first reported in 2004.[13] CDs are zero-dimensional (0D) carbon or 0D carbon-based nanomaterials.[14-18] Due to their excellent optical properties, low toxicity, good biocompatibility, environment-friendly, and facile preparation, and has shown exciting advantage in various application fields. [19, 20] Due to the variety of synthesis routes (top-down and bottom-up) and the abundance of raw materials (graphite, small organic molecules, polymers, and natural materials), a variety of CDs have mushroomed. The abundance of precursors, synthesis methods, and unknown reaction processes increase the difficulty of elucidating precise chemical structure of CDs. Researchers have tried to classify and name different CDs according to their structure and performance characteristics, but there is still a wide range of debate.[21-23] The formation of CDs mainly involves the aggregation of C, N, and O elements.[24-27] The proportions of these elements vary greatly among different types of CDs. The conjugated carbon  $sp^2$  domains (chromophores) inside CDs are proposed to have planar fused aromatic ring structures similar to fluorescent organic molecules.[28] Similar to organic fluorescent

molecules, most of the initially synthesized CDs showed an aggregation-induced quenching effect. However, later research revealed that some CDs showed aggregation-induced (i.e. enhanced) luminescence, including concentration dependent luminescence<sup>[29-31]</sup> and solid-state luminescence.<sup>[32-34]</sup> In both the synthesis of CDs and their emission characteristics, aggregation plays an important role. Understanding such aggregation processes is of vital importance when designing CDs for particular applications.

This review aims to summarize recent research relating to synthesis and optical properties of CDs, placing particular emphasis on the role of aggregation in the formation of different kinds of CDs, including graphene quantum dots (GQDs), carbon quantum dots (CQDs), and carbonized polymer dots (CPDs), and subsequently how the aggregation of CDs with specific morphologies can realized special luminescent properties (Scheme 1).

## 2. Aggregation in different types of CDs

CDs are a general term for 0D carbon nanomaterials. However, owing to the diversity of their nanostructures, it is difficult to accurately define and classify them, resulting in widespread debate. At present, CDs can be roughly divided into three categories: GQDs, CQDs and CPDs (Figure 1A). Aggregation is a crucial part of the formation of each type of CDs.<sup>[21, 23]</sup> The aggregation of elements in CDs formation is very different for each. The aggregation of elements in CDs formation is very different for each. Below we examine the formation process, structure, classification of GQDs, CQDs and CPDs.

### 2.1. GQDs

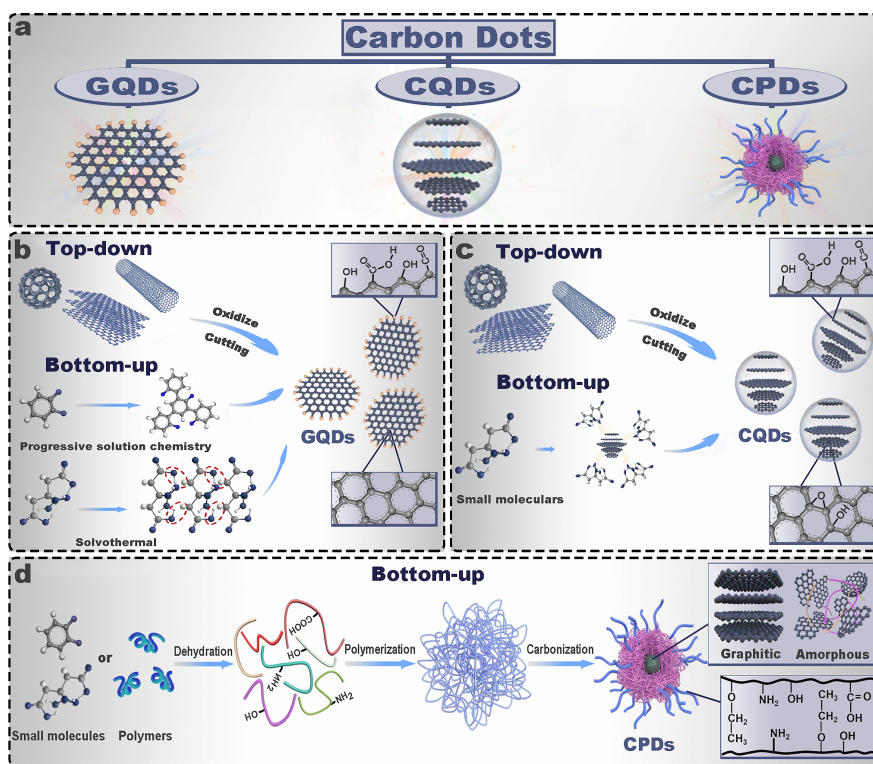


**Figure 1 .** (A) Classification of CDs as GQDs, CQDs, or CPDs. (B) Schematic diagram of GQDs synthesis. (C) Schematic diagram of CQDs synthesis. (D) Schematic diagram of CPDs synthesis.

GQDs were first prepared by Ponomarenko et al.<sup>[35]</sup> in 2008 based on the previous report on CDs by Xu et al.<sup>[13]</sup> in 2004. GQDs can be regarded as a subset of graphene and/or graphene oxide with  $sp^2$  structure, exhibiting similar chemical and physical properties to it. However, unlike two-dimensional graphene sheets

with zero band gap, the GQDs is typically anisotropic characterized by single or less layers atomic graphite planes with lateral size typically  $<10$  nm. The bandgap of GQDs is opened due to the quantum confinement effects caused by the small size, and is closely related to the size (mainly refers to the conjugated  $sp^2$  domain), which is the major feature of GQDs.<sup>[36]</sup> Density functional theory (DFT) calculations have shown that the bandgaps of GQDs decrease from around 7 eV for benzene to 2 eV for GQDs consisting of 20 fused aromatic rings.<sup>[37]</sup> Moreover, the photoluminescence (PL) of GQDs can be precisely regulated by control of the attached chemical functionalities, heteroatom doping, defects, edge configuration, and shape.<sup>[38, 39]</sup> Many regard GQDs as giant polyaromatic molecules.<sup>[40]</sup> Compared to simple polyaromatic molecules, GQDs are more complex in that they are larger, carry abundant functional groups, and have narrower and more complex band gap structures. The intense PL emissions of GQDs can be roughly divided into two primary types: PL originating from created or induced energy bandgaps in single sheet GQDs and PL that is associated with defects in single- and/or multiple-layer graphene. There are many different opinions about the number of layers in GQDs, with 1-3 layers,<sup>[41]</sup>  $<5$  layers,<sup>[42]</sup> or  $<10$  layers being advocated in different literature. In the discussion below, we mainly focus on GQDs with less than 5 layers (GQDs with more layers are classified as CQDs in the current work).

There are two types of synthetic routes towards GQDs: top-down and bottom-up methods (Figure 1B). The top-down method involves controlled fragmentation of bulk carbonaceous materials (e.g., graphite, graphene sheets, carbon nanofibers, and carbon nanotubes) into small pieces. The most commonly used methods include oxidative/reductive cutting,<sup>[39, 43]</sup> physical grinding,<sup>[44]</sup> or combination of cutting and grinding.<sup>[45]</sup> Top-down methods have the advantages of abundant raw materials, simple operation, and large scale production, but do not allow accurate control over the size and morphology.<sup>[46]</sup> The formation of GQDs by top-down methods does not involve the aggregation of precursors. Accordingly, the C:H ratio in GQDs prepared by top-down methods is typically near-unity, with C mainly existing in  $sp^2$  form. However, top-down preparation methods result in partial oxidation of some carbons, whilst also introducing certain functional groups (e.g. hydroxyl, carbonyl, carboxylic acid, and epoxy/ether groups) and/or doping of heteroatoms into the GQDs. These surface modifications give GQDs good dispersibility, with the introduced defects often acting as fluorescent centers into the GQDs.<sup>[47]</sup>  $\pi$ - $\pi$  stacking interactions between adjacent layers in GQDs can cause interlayer quenching, similar to that seen for large conjugated aromatic hydrocarbons or conjugated fluorescent polymers. The effect of such “aggregation” on the optical properties of GQDs is explored in section 4.

Compared with the top-down methods, synthesis of GQDs by bottom-up methods is more chemically challenging, but allows the preparation of GQDs with more uniform morphologies and controlled size. Progressive reaction in solution is the dominant approach for the bottom-up synthesis of GQDs. In such bottom-up methods, aggregation is critical to the synthesis of GQDs, with the aggregation of precursors being a critical initial step. Such methods have more stringent precursor requirements, typically utilizing molecules with conjugated structures or molecules that combine to form six-membered rings, such as hexabromobenzene [48], hexa-peri-hexabenzocoronene,<sup>[49]</sup> 1,3,6-trinitropyrene,<sup>[50]</sup> citric acid (CA),<sup>[51]</sup> glucose,<sup>[52]</sup> and so on. The reaction precursors react and aggregate into larger graphene-like sheets, with aggregation controlling the lateral size and thickness (number of layers). Most GQDs prepared by such routes are anisotropic. Liu et al.<sup>[49]</sup> used hexa-peri-hexabenzocoronene as precursor to prepare GQDs through a stepwise process of aggregation, carbonization, oxidization, surface functionalization, and reduction (Figure 2A). Wide-angle X-ray scattering show that the unit cell parameter of the GQDs was consistent with the length of the hexa-peri-hexabenzocoronene molecule, with a strong diffraction peak observed attributed to the  $\pi$ - $\pi$  stacking distance between two overlapped molecules of hexa-peri-hexabenzocoronene. Moreover, by performing control experiments using hexa-peri-hexabenzocoronene derivatives with different functional groups, it was demonstrated that the condensed stacking of hexa-peri-hexabenzocoronene in the GQDs could be attributed to the lack of steric hindrance from the substituents, leading to the generation of graphitic framework with few defects during the carbonization step. Lee et al.<sup>[52]</sup> prepared GQDs through catalytic solution chemistry (Figure 2B). The D-glucose carbon source aggregated horizontally through spontaneous dehydration, resulting in the formation of graphene. Dong et al.<sup>[51]</sup> similarly developed the synthesis of monolayer GQDs using a

CA precursor (Figure 2C). Yan et al. <sup>[53, 54]</sup> reported the preparation of GQDs with a tunable size through solution chemistry (Figure 2D) involving surface modification with 2, 4, 6-triakyl phenyl. This synthesis route allowed accurate control of the number of conjugated carbon atoms. Crowdedness at the edges of the graphene cores caused twisting of the phenyl groups of 2, 4, 6-triakyl phenyl away from the plane of the core, leading to alkyl chains projecting in all dimensions. This reduces the face-to-face interaction between the developing graphene sheets, allowing large GQDs to be synthesized with good solubility.

For all of the aforementioned GQDs, the band gap is closely related to the size (especially the size of the  $sp^2$  domain) and number of layers resulting from aggregation. Yeh et al.<sup>[55]</sup> showed that the band gap in GQDs decreased with increasing GQDs lateral size (Figure 2E). The PL color varied from red-orange to blue as the GQDs size was reduced (from 8 to 1 nm). Results are consistent with quantum confinement with decreasing size in the  $sp^2$  conjugate domains. Dong et al.<sup>[56]</sup> prepared GQDs by chemically oxidizing CX-72 carbon black (Figure 2F). This synthesis route produced monolayer and multi-layer GQDs simultaneously, with sizes of 15 nm and 18 nm, respectively. Monolayer and double-layer GQDs have strong green and yellow PL emissions, respectively. Yan et al. <sup>[57]</sup>proposed two different strategies to narrow down the electronic band gap of GQDs (Figure 2G). Since the band gap of pristine GQDs is negatively correlated with the size of the  $sp^2$  domain, bandgap narrowing was realized via conjugating GQDs with polyaromatic molecules to enlarge the  $sp^2$  carbon network. The sensitivity of GQDs to this type of modification is due to the anisotropy and small size of GQDs. This strategy may not work well for other types of CDs whose bandgaps are less sensitive to quantum confinement effects.<sup>[40]</sup>

## 2.2. CQDs

Fluorescent carbon nanoparticles were first named CQDs by Sun et al. in 2006 <sup>[58]</sup>. Like GQDs, CQDs also have quantum confinement and crystalline core structures. The main different between GQDs and CQDs is their shape and core composition. GQDs are anisotropic with crystalline  $sp^2$  cores, whereas CQDs are quasi-spherical carbon nanoparticles with less crystallinity and containing more defects. CQDs typically possess as crystalline core containing a mixture of  $sp^2$  and  $sp^3$ carbons. Usually, CQDs are terminated by oxygenic/nitrogenous functional groups, with heteroatom contents ranging from 5-50 wt.%. The differences between GQDs and CQDs mainly originate from the different precursor aggregation pathways in their respective syntheses.

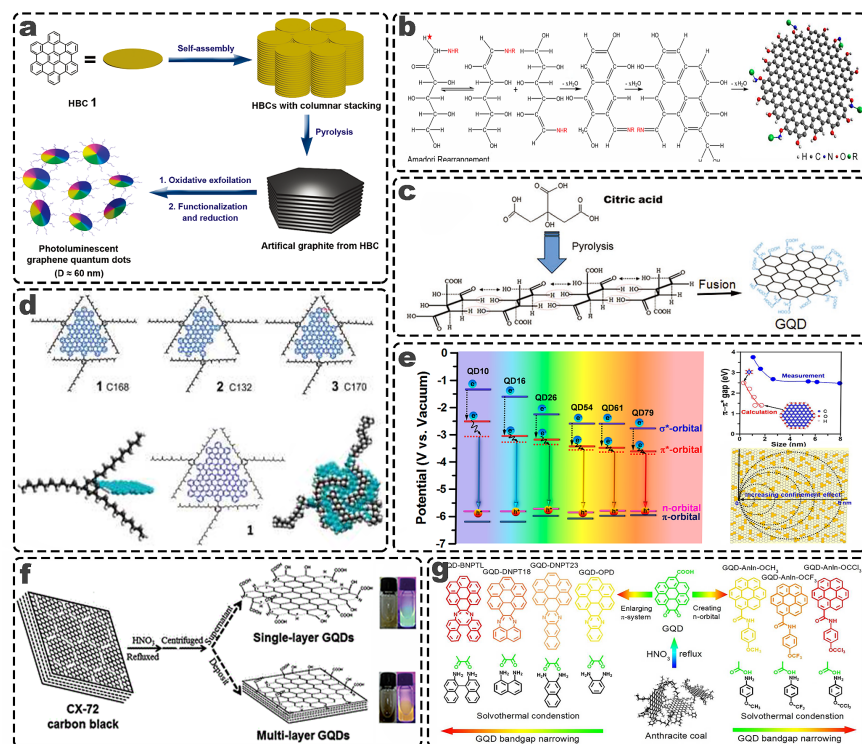


**Figure 2.** (A) Fabrication of GQDs via a soft-template method based on Hexa-peri-hexabenzocoronene as the carbon source. Reproduced with permission.<sup>[49]</sup> Copyright 2011, American Chemical Society. (B) Schematic diagram of GQDs synthesized by catalytic solution chemistry using glucose. Reproduced with permission.<sup>[52]</sup> Copyright 2019, American Chemical Society. (C) Pyrolysis technique for producing GQDs using CA as a raw material. Reproduced with permission.<sup>[51]</sup> Copyright 2012, Elsevier. (D) Solubilization strategy towards colloidal GQDs using 2, 4, 6-trialkyl phenyl groups. Reproduced with permission.<sup>[53]</sup> Copyright 2010, American Chemical Society. (E) Schematic energy level diagram for GQDs specimens and quantum confinements introduced in the  $sp^2$  domain. Reproduced with permission.<sup>[55]</sup> Copyright 2016, American Chemical Society. (F) The synthetic route towards GQDs from CX-72 carbon black. Reproduced with permission.<sup>[56]</sup> Copyright 2012, Royal Society of Chemistry. (G) Illustration of band gap narrowing by enlarging the  $\pi$ -conjugated system via conjugating GQDs with poly-aromatic rings or by introducing an intermediate n-orbital level in the band gap via conjugating with electron-donating groups. Reproduced with permission. Reproduced with permission.<sup>[57]</sup> Copyright 2018, American Chemical Society.

As with GQDs, CQD can be synthesized by top-down and bottom-up routes (Figure 1C). Methods for preparing the CQDs by top-bottom routes are similar to those described for GQDs and does not involve the aggregation of precursors. Tao et al. <sup>[59]</sup> obtained three different CQDs from graphite, single-walled carbon nanotubes and multi-walled carbon nanotubes, respectively, using acid treatments (Figure 3A). Due to the mixed  $H_2SO_4/HNO_3$  treatments, the obtained CQDs possessed a high oxygen content (up to 55%). TEM and AFM images shown that all CQDs samples consisted of spherical nanoparticles. The fluorescence emission of the CQDs is attributed to the poly-aromatic  $sp^2$  carbon nanostructures, as well as the various functional groups on their surface. Hu et al.<sup>[60]</sup> synthesized CQDs by laser irradiation of graphite flakes in polymer solution. By regulating the laser pulse width, cavitation bubbles of various sizes and densities were formed, leading to CQDs of different sizes (Figure 3B). After a laser pulse, nuclei/clusters were first formed. As the cavitation bubbles shrunk, the nuclei/clusters were forced to interact with aggregation creating CQDs.

For the bottom-up synthesis of CQDs, the most commonly used methods are microwave methods, thermal decomposition, and hydrothermal methods. Unlike GQDs, the precursors aggregate by dehydration to form

tiny spherical nuclei. The remaining reaction precursors then further aggregate on the surface of the initially formed nuclei, eventually forming CQDs. Tang et al. [61] prepared CQDs using glucose as a precursor using a hydrothermal method (Figure 3C). TEM and AFM showed the diameter and height of the CQDs to  $3.4 \pm 0.5$  nm and 3.2 nm, respectively, confirming a near spherical structure.

The bottom-up formation process of CQDs typically involved the following steps: Precursors are first dehydrated to form C=C-containing nuclei. Additional precursor molecules then deposit on the surface of the nuclei and generate new C=C bonds by dehydration. By this pathways, spherical CQDs and formed which becomes larger as the reaction time increases (assuming precursor remains available). Ma et al. [62] showed that intermediates produced during ethylene diamine tetraacetic acid decarboxylation gradually fused together to give graphite-like structures (CQDs) under the solid-state reaction conditions (Figure 3D), with the same compounds being converted into graphitic carbons at much higher pyrolysis temperatures.

The PL of CQDs is affected by quantum confinement effects and also size, functional groups, and edge effects. [63] Surface defects formed by surface oxidation can capture excitons and generate fluorescence associated with surface-states. With the increase of surface oxidation degree of CQDs, more surface defects were formed. This results in a narrowing of energy levels and a redshift in PL emission. Single sheets are often required for band gap PL emissions in graphene-based materials in order to restrain interlayer quenching. However, the single sheet requirement does not hold for defect-origin fluorescence [64] in quasi-spherical CQDs. Wang et al. demonstrated that CQDs tend to have green PL centers, attributed to edge states (carbon atoms on the edge of carbon backbone and functional groups that include C=O like carbonyl and carboxyl groups). They found that competition between the emission centers (edge states) and the traps control the optical properties of CQDs. [65]

### 2.3. CPDs

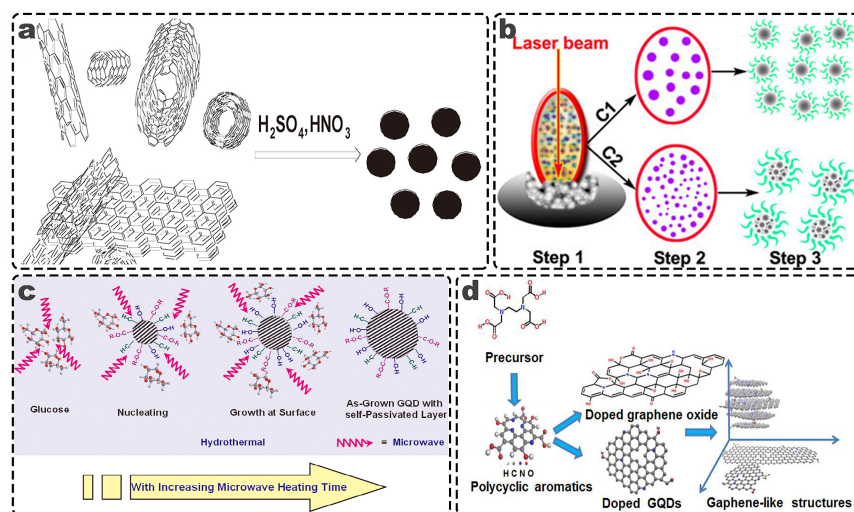


**Figure 3.** (A) Synthesis of CQDs from various carbon sources. Reproduced with permission. [59] Copyright 2012, Wiley-VCH. (B) Schematic of the mechanism of size control of CQDs obtained upon laser ablation in poly(ethylene glycol) liquid. Reproduced with permission. [60] Copyright 2011, Springer. (C) Preparation of GQDs by a microwave-assisted hydrothermal (MAH) method. Reproduced with permission. [61] Copyright 2012, American Chemical Society. (D) Schematic illustration of the reaction process for preparation of GQDs from EDTA (E-GQDs) and their graphene-like structures. Reproduced with permission. [62] Copyright 2015, Royal Society of Chemistry.

CPDs was first proposed by Yang et al [42, 66] in 2018, and since that time have attracted extensive research interest and attention. CPDs are transitional materials between polymer dots and fully carbonized

materials.<sup>[67]</sup> Since their synthesis involves both polymerization and carbonization processes, CPDs offer a rich platform towards luminescent carbon-based nanomaterials.<sup>[68]</sup> CPDs has a unique polymer/carbon hybrid structure and special PL mechanisms.<sup>[69]</sup> Not surprising, the properties of CPDs are quite distinct from GQDs, CQDs and polymer dots. The polymeric component of CPDs confers three advantages: (1) abundant functional groups and short polymer chains resulting from incomplete carbonization, (2) polydispersity in CPDs structure, (3) and highly crosslinked network structure generated by the process of dehydration and carbonization.<sup>[70]</sup> Crosslink-enhanced emission (CEE) is a unique PL property of CPDs, which can be further divided into covalent-bond CEE and noncovalent-bond CEE (supramolecular-interaction CEE, ionic-bonding CEE and confined-domain CEE).<sup>[71]</sup>

CPDs synthesized by the carbonization of PDs by bottom-up methods usually have no clear boundary between the core and shell (Figure 1D). The carbon core of CPDs can exhibit intrinsic state or subdomain state emission.<sup>[72]</sup> Typically the core comprises a paracrystalline carbon core structure composed of tiny carbon clusters surrounded by polymer frames,<sup>[73]</sup> or instated partially dehydrated and carbonized crosslinked chains.<sup>[70]</sup> Tiny carbon clusters as the subdomain in the carbon core can adopt conjugated  $\pi$ -structures or diamond-like structure, with the conjugated  $\pi$ -structure being planar or curved (e.g. fullerene-like fragments).<sup>[74]</sup> Further, CPDs can also be synthesized by the post-synthetic decoration of CQDs with polymers or organic molecules. The CPDs synthesized by post-synthetic-decoration possess a well-defined boundary between the core (CQDs) and the polymer shell.

The precursors used to synthesize CPDs are extensive, with many organic molecules forming CPDs through hydrothermal cross-linking polymerization.<sup>[42]</sup> Since most of the precursors are asymmetric, intermolecular aggregations during dehydration lead to the formation of long polymer chains with a certain degree of crosslinking.<sup>[75]</sup> In such cases, the aggregation of the precursors is highly disordered. As the hydrothermal temperature rises, condensation, crosslinking and polymerization reactions occur in the chain segments of the preformed polymer chains, generating numerous random coils.<sup>[74, 76]</sup> Due to the shortened spatial distance, crosslinking further proceeds in the interior of polymer clusters and the structures get more compact and stable over time, resulting in CPDs with a small degree of carbonization. In the latter stages of the reaction, the polymeric fraction is reduced with a concomitant increase in the carbonization degree, leading to microcrystalline carbon regions in the interior of CPDs.<sup>[77, 78]</sup> Yang et al. <sup>[79]</sup> studied the structural evolution of CPDs (Figure 4A). CPDs with different emitting wavelengths were synthesized from CA-like precursors and ammonia, with the formation of CPDs involving three different stages. Taking CA as a representative example, CA and ammonia first form a six-membered ring molecules through amidation reactions. The  $\pi$ -conjugated domain of the ring systems were further extended through intermolecular amination, deacidification, and dehydration. Next, the intermediate products were further dehydrated to form a polymer. Finally, the polymers were further dehydrated and carbonized into CPDs. They also found that the carbon chain length of CA-like starting molecules controlled the cyclization mode, resulting in hexatomic, pentatomic, unstable four/three-membered ring systems or cyclization failure. CA-like starting molecules that formed hexatomic rings in the initial stages resulted in CPDs with the largest emission redshift. Shamsipur et al. <sup>[74]</sup> exhibited the existence of three different emission centers in CDs prepared through pyrolysis of CA and ethylenediamine (Figure 4B). These emission centers included molecular states, conjugate domain states, and carbon-core states. During dehydration processes at low temperatures, cyclization and polymerization of the raw materials generated highly fluorescent polymeric-like structures with a strong PL. The PL originated from molecular fluorophores incorporated in polymer structures. Further dehydration resulted in the growth of more  $\pi$ -conjugated structures (including polycyclic aromatic hydrocarbons, fullerene fragments, and even more complex aromatic structures) within the polymeric structures. Further carbonization generated nano-sized CPDs with carbon-cores, but the CPDs still contained fluorophore molecules associated with different aromatic domains. Wang et al. <sup>[80]</sup> explored the aggregation process of six different CPDs prepared with conjugated precursor o-phenylenediamine (Figure 4C). After being protonated by acid, aggregation was reported to take place in two ways: lateral growth (formation of long linear polymer chains) and longitudinal (formation of wide conjugated planar fragments). According to the calculated formation energies, the lateral growth needed much higher energies than longitudinal growth. The results revealed that

o-phenylenediamine tends to aggregate into planar structures, then self-assemble into spherical CPDs with the polymer stacking inside the core being different from the surface polymer shell. The tangled polymer core more rapidly underwent dehydration and carbonization. The latter is the key to obtain highly photoluminescent CPDs from polymers without intrinsic fluorescence. Xia et al. [81] reported the nucleation process of CPDs was similar to the soap-free emulsion polymerization (Figure 4D). Firstly, the aggregation leads to the formation of polymer clusters. After dehydration and crosslinking, the hydrophobicity of the polymer clusters increases, leading to the internal hydrophobic structure and external hydrophilic structure, with the microphase separation aiding the formation of the carbon core.

A clear understanding of the CDs structure is essential to understanding the formation process of CDs and structure-property relationships. Owing to their small size and presence of heteroatoms, accurate structural information about CDs is difficult to obtain. This makes the main force driving their construction also uncertain. Recently, many researchers have started from the perspective of a single crystal, then tried to extend this model to capture the precise structure of CDs. Yang et al. [82] reported the successful synthesis of a new kind of crystalline luminescent organic nanodot by kinetically trapped self-assembly, which was then applied for a simplified  $\pi$ -packing model to simulate the structure of CDs (Figure 4E). The precise aggregation and structure induced PL of the nanodots allowed structural-property relationships between the nanodots and single crystal CDs to be established. This study shows that crystalline organic nanodots with precise structures provide a solid platform for exploring the structure of CDs.

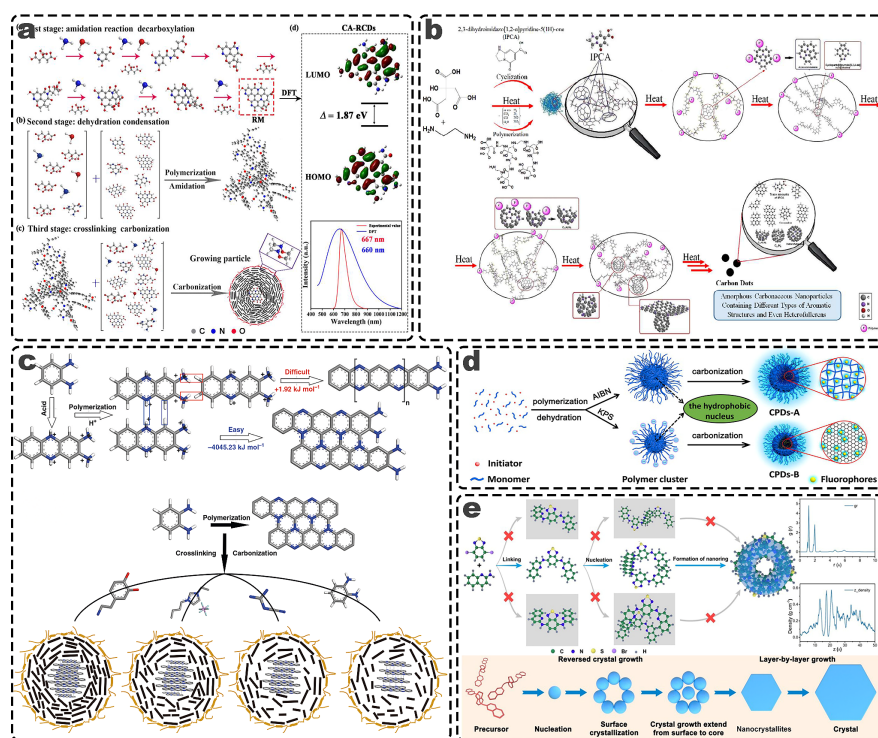


**Figure 4.** (A) Schematic diagram of CPDs formation process. Reproduced with permission. [79] Copyright 2022, Elsevier. (B) Schematic representation of the formation of CPDs from citric acid and ethylenediamine through a pyrolysis process. Reproduced with permission. [74] Copyright 2018, American Chemical Society. (C) Formation process and structural analysis of CPDs. Reproduced with permission. [80] Copyright 2022, Springer. (D) Schematic diagram of the nucleation and reaction process leading to CPDs. Reproduced with permission. [81] Copyright 2018, Wiley-VCH. (E) Schematic diagram of the crystallization mechanism of hexagonal crystals driven by kinetically trapped self-assembly. Reproduced with permission. [82] Copyright 2022, Wiley-VCH.

### 3. Aggregation in different types of CDs

The physical and chemical properties of nanoparticles are closely related to their morphology. A wide range of inorganic nanoparticles can be synthesized with well-defined morphologies, which typically involves regulating the crystal growth conditions. Morphology-engineering creates new properties, opening the door to new applications.<sup>[83-85]</sup> However, the morphology of CDs is often difficult to achieve owing to the ways they are synthesized (i.e. by rapid top-down or bottom-up strategies), hindering the further development of CDs.

As mentioned above, GQDs are typically anisotropic composed of single or multi-layer sheets, whereas CQDs and CPDs are spherical or quasi-spherical. A few studies have reported the synthesis of GQDs and CQDs with novel morphologies. However, the morphology of CPDs is especially difficult to change. In GQDs and CQDs, the aggregation of precursors occurs horizontally or vertically, while in CPDs, the aggregation of precursors is disorderly and random. Therefore, the aggregation in the synthesis of GQDs and CQDs is easier to control. Yuan et al.<sup>[86]</sup> used phloroglucinol as precursors to synthesize triangular CQDs of different sizes (Figure 5A). The raw material phloroglucinol possesses a unique molecular structure with three highly reactive hydrogen atoms at the three meta positions activated by three electron-donating hydroxyl groups, which was crucial for the synthesis of the triangular CQDs. Subedi et al.<sup>[87]</sup> reported the synthesis of anisometric CQDs using rigid-rod-shaped precursors (Figure 5B). Meng et al.<sup>[88]</sup> successfully obtained carbon quantum rings exploiting terephthalaldehyde and p-phenyldiacetonitrile as precursors (Figure 5C). The two precursor molecules undergo specific aggregation to form ribbons of different lengths. Cyano groups at the edges promoted curvature of conjugated aromatic carbon ribbons, forming carbon quantum rings with different diameters. To date, there has only been only one report demonstrating morphology-engineering of CPDs. Xiong et al.<sup>[89]</sup> synthesized carbon nanorods by a reverse micellar method (Figure 5D). First, aminopropylisobutyl polyhedral oligomeric silsesquioxane and citric acid self-assembled into complex structures (CPDs) in a nonpolar solvent, with the citric acid fraction in the assemblies then aggregating and carbonizing to form carbon nanorods.

In addition, the aggregation caused by the interaction between CDs leads to assemblies with different morphologies. Li et al.<sup>[90]</sup> first explored the mechanisms involved in the aggregation of multiple GQDs (Figure 5E). First, protonation/deprotonation of GQDs at different pH values caused GQDs to self-assemble into GQDs-water-GQDs units. Additionally, GQDs can assemble into large plates in the presence of  $\text{Ca}^{2+}$ , which then convert into three-dimensional structures via  $\pi$ -p stacking. Ba et al.<sup>[91]</sup> prepared spherical arrays of CDs for solid state luminescence.

### 4. Special luminescence phenomenon of CDs caused by aggregation

In the previous section, we discussed the aggregation of different types of CDs in detail. When aggregation occurs between particles, their interactions can lead to special luminescence phenomena. In this section, we discuss these special luminescence phenomena resulting from CDs aggregation.

#### 4.1. Aggregation induced fluorescence quenching and quench-resistant

Aggregation induced fluorescence quenching describes the phenomenon wherein a fluorophore has effective luminescence in dilute solution, but the fluorescence is reduced or even disappears completely in concentrated solution or the solid state.<sup>[10, 92]</sup> Most CDs show this phenomenon, due to the quenching effect and reabsorption effect at high concentrations. Hence, beyond some threshold (low) concentration, the PL intensity of CDs decreases with an increase of concentration. The aggregation induced fluorescence quenching effect of small organic luminescent molecules with planar aromatic ring structures is described as follows: when they are close enough, their large planar polycyclic aromatic structure encourages make them orientate due to strong intermolecular  $\pi$ -p stacking interactions. This superposition of molecules will allow the photoexcited state to fall back to the ground state via the nonradiative transition, resulting in luminescence quenching. It reasonable to assume that in CDs with similar planar aromatic ring structures, a similar quenching process occurs as the concentration increases. Due to the complex structure of CDs, multiple quenching mechanisms may be possible and the origin of the quenching difficult to identify.

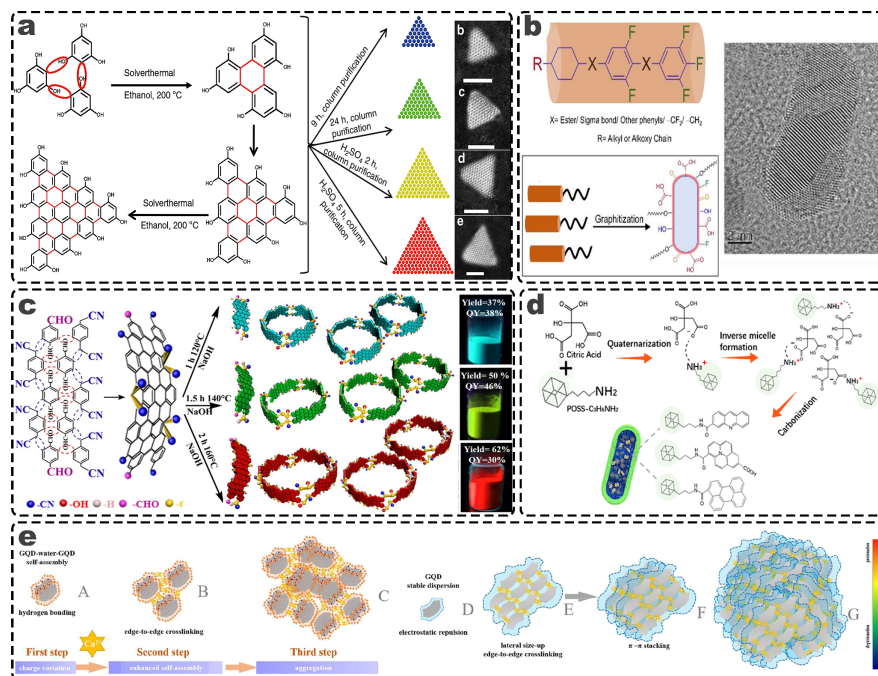


**Figure 5 .** (A) Solvothermal route towards triangular CQDs. Reproduced with permission.<sup>[86]</sup> Copyright 2018, Springer. (B) Schematic illustration of the in-situ synthesis of CQDs. Reproduced with permission.<sup>[87]</sup> Copyright 2022, American Chemical Society. (C) Schematic illustration of the synthesis of annular CQDs. Reproduced with permission.<sup>[88]</sup> Copyright 2021, Wiley-VCH. (D) Scheme showing inverse micelle formation and carbonization process during carbon nanorod synthesis. Reproduced with permission.<sup>[89]</sup> Copyright 2019, American Chemical Society. (E) Proposed three-step mechanism for the aggregation behavior of GQDs with and without the addition of salt under acidic (protonation) and alkaline (deprotonation) conditions. Reproduced with permission.<sup>[90]</sup> Copyright 2017, American Chemical Society.

For small organic fluorophore molecules, aggregation is often prevented by introducing steric hindrance or through molecular conformation control. For example, by connecting bulky rings, spiral kinks, and dendritic wedges covalently to aromatic cores, intermolecular  $\pi$ - $\pi$  stacking interactions can be avoided.<sup>[28, 93]</sup> Similar methods have also been used to restrain the aggregation induced fluorescence quenching of CDs.<sup>[94]</sup> Park et al.<sup>[95]</sup> exhibited that surface functionalization of GQDs with hexadecylamine, poly(ethylene glycol), and polyhedral oligomeric silsesquioxane could reduce  $\pi$ - $\pi$  stacking-induced the fluorescence quenching of GQDs (Figure 6A). Li et al.<sup>[96]</sup> prepared carbon nanorings using elaborate precursors and synthesis processes that effectively suppressed aggregation induced fluorescence quenching.

In addition, embedding CDs in the matrix is further approach to prevent aggregation. Commonly used substrates are polymers, acid molecules condensates, inorganic salts, organic-inorganic hybrid materials, and mesoporous or layered materials.<sup>[97]</sup> Park et al.<sup>[98]</sup> incorporated GQDs within a boron oxynitride matrix, with aggregation induced fluorescence quenching being significantly suppressed. Zhou et al.<sup>[99]</sup> reported strongly luminescent CDs@silica composite gels, with the gel matrix hindering collision between high concentrated CDs (Figure 6B).

#### 4.2. Aggregation-induced emission

Aggregation-induced emission (AIE) refers to fluorophores that have negligible light emission in the dilute solution, but strong emission in aggregated form.<sup>[100]</sup> In studies of small organic molecules, AIE can be achieved in many ways, especially in cases where aggregation limits intramolecular rotation, aggregation limits intramolecular vibration, or highly twisted aggregated structures weaken intermolecular  $\pi$ - $\pi$  stacking.<sup>[92]</sup>

In CDs, phenomena similar to AIE have been reported, specifically aggregation-induced fluorescence enhancement and aggregation-induced wavelength-redshifts. In a large degree, concentration-dependent PL is a reflection of AIE in CDs. Liu et al.<sup>[101]</sup> prepared CDs using tannic acid, which exhibit visual aggregation induced emission enhancement. The enhancement was attributed to surface groups on the CDs, such as aromatic rings and phenolic hydroxyl (Figure 6C), interacting to hinder rotation in the fluorophores. Many researchers have proposed that aggregation increases the conjugation degree of surface luminophores, leading to a decrease of band gap. Hence, emission wavelengths gradually red shift with increasing CDs concentration. Yang et al.<sup>[102]</sup> designed CPDs from dithiosalicylic acid/acetic acid and melamine (Figure 6D). The CPDs contained two PL centers,  $\pi$ -conjugated domains in the nucleus, and S–S bond on the surface. In the dispersed state, the S–S bond did not possess fluorescence emission due to intramolecular rotation, with the blue emission of  $\pi$ -conjugated domains dominating the emission spectrum. When the CPDs aggregate, the  $\pi$ -conjugated domains undergo  $\pi$ – $\pi$  stacking, quenching the blue emission. However, aggregation causes rotation restriction of S–S bonds, resulting in a red emission. Unlike extremely low quantum yields caused by H-type aggregation, J-type aggregation usually results in a red-shift of the emission wavelength. Chen et al.<sup>[103]</sup> and Li et al.<sup>[104]</sup> both developed GQDs exhibiting red-shift emissions at high concentration, involving self-assembled J-type  $\pi$ -p aggregates. They indicated that the large number of carboxyl groups at the edge of GQDs are limit  $\pi$ -p intermolecular interactions, thus leading to J-type aggregation rather than H-type aggregation.

### 4.3. Aggregation-induced room temperature phosphorescence

Aggregation often causes another special phenomenon to emerge, such as room temperature phosphorescence. Phosphorescence is more difficult to produce than fluorescence because it involves a triplet exciton transition and is spin-forbidden.<sup>[108, 109]</sup> At room temperature, the long lifetime of the triplet excitons means they are easily dissipated by nonradiative decay processes.<sup>[110]</sup> In order to produce phosphorescence, efficient intersystem crossing and suppression of nonradiative transitions are necessary. Hence, the room temperature phosphorescence of CDs is usually realized in the aggregate state, which can strongly limit fluorescence and promote radiative relaxation via phosphorescence. Lin et al.<sup>[105]</sup> prepared room temperature phosphorescence CDs via hydrothermal treatment of trimellitic acid (Figure 6E). Aggregates of the large conjugated structures created a triplet excited state resulting in aggregation-induced phosphorescence. The abundant sub-luminophores supply sufficient energy levels contributing to populate triplet states via intersystem crossing. Crosslinked polymer networks can also effectively protect fluorophores and inhibit nonradiative transitions. Yang et al.<sup>[106]</sup> demonstrated that the covalent crosslinking in the interior of CPDs can prevent the vibrations and rotations of polymer chains, thus providing favorable conditions for intersystem crossing (Figure 6F). Through hydrothermal addition polymerization with acrylamide as monomer, they synthesized ultrahigh-yield CPDs with ultralong phosphorescence lifetime. Carbonization changes the degree of crosslinking and forces the sub-luminophores to form aggregates that increase the degree of conjugation, leading to an emission red-shift. Likewise, inspired by the concept of CEE. Wang et al.<sup>[107]</sup> prepared CPDs with room temperature phosphorescence by self-crosslinking and carbonization (Figure 6G). The core-shell structure of CPDs enhanced the crosslinking of CPDs and boosted the phosphorescence, creating rich energy levels for intersystem crossover. They proposed a design rule that can be applied for adjust the quantum yields and phosphorescence lifetime of CPDs, based on the stabilization of triplet excited states through the degree of crosslinking.

## 5. Application

Aggregation not only affects the morphology and luminescence of CDs, but also creates special applications for CDs.

### 5.1. Anti-counterfeiting applications

Security inks and labels containing fluorophores are increasingly being used to identify counterfeit products. CDs with solid-state PL show great potential for anti-counterfeiting. The surface of CDs is rich in hydrophilic functional groups, enabling CDs-based inks to be inkjet printed on paper with good adhesion. The different

PL wavelength and long-life afterglow of solid-state PL, room temperature phosphorescence and delayed fluorescence materials based on CDs offers double or even triple anti-counterfeiting protection. Jiang et al.<sup>[111]</sup> printed a portrait of Chairman Mao onto a banknote utilizing CDs (Figure 7A). The CDs were colorless under ambient conditions, but showed a blue emission and under 365 nm ultraviolet light. When the excitation light was off, the printed portrait showed green phosphorescence. Tao et al.<sup>[106]</sup> developed a dual-mode anti-counterfeiting material. A colorful butterfly was drawn using commercial fluorescent materials and long-life afterglow CDs. Under UV light, the butterfly pattern possessed multicolor fluorescence. However, on turning off the UV lamp, a green phosphorescence appeared in the encrypted part of the butterfly. In another multi-mode example<sup>[112]</sup>, adding CDs to a printer's color ink can cause afterglow emission to appear in the given area of the printed pattern, thus achieving multi-mode anti-counterfeiting. Furthermore, CDs can also be utilized in fingerprint analysis. When the finger touches something, oily sebum and sweat will leave a latent fingerprint, which is not visible to the naked eye and needs to be enhanced. Chen et al.<sup>[113]</sup> prepared red emission CDs for this purpose, with the red emission negating potential background fluorescence interference from fluorophores in the fingerprints. A coffee ring effect and electrostatic interaction overcame the aggregation-induced fluorescence quenching of CDs. Dong et al.<sup>[114]</sup> combined CDs and starch to prepare phosphors on a large scale (Figure 7B). A digital processing program was applied to objectively identify the latent fingerprint, with a high degree of matching.

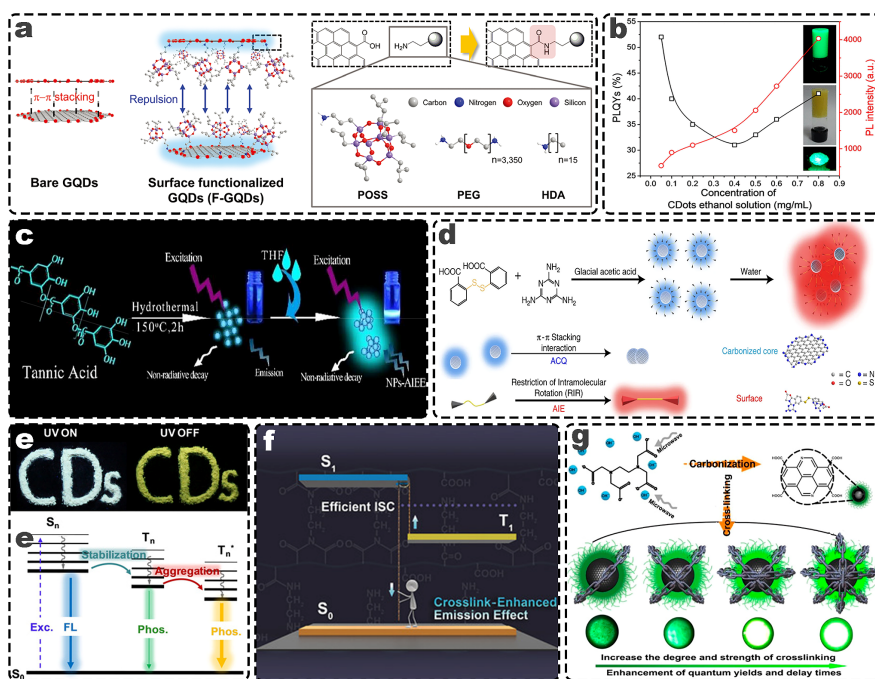


**Figure 6 .** (A) Schematic illustration of quenching-resistant photoluminescence of surface-functionalized GQDs. Reproduced with permission.<sup>[95]</sup> Copyright 2021, Wiley-VCH. (B) Quantum yield and PL intensity at different concentrations of CDs. Reproduced with permission.<sup>[99]</sup> Copyright 2017, American Chemical Society. (C) Schematic of the synthesis of CDs and the CDs aggregation induced emission enhancement effect caused by tetrahydrofuran. Reproduced with permission.<sup>[101]</sup> Copyright 2015, Royal Society of Chemistry. (D) Formation of CDs monomers and their aggregates. Reproduced with permission.<sup>[102]</sup> Copyright 2019, Springer. (E) Fluorescence and phosphorescence processes of CDs powder at ambient conditions. Reproduced with permission.<sup>[105]</sup> Copyright 2019, Wiley-VCH. (F) Schematic diagram of crosslink-enhanced emission effect leading to the generation of room temperature phosphorescence. Reproduced with permission.<sup>[106]</sup> Copyright 2019, Wiley-VCH. (G) Proposed room temperature phosphorescence mechanism of CDs with different degrees of crosslinking. Reproduced with permission.<sup>[107]</sup> Copyright 2022, Wiley-VCH.

## 5.2. Anti-counterfeiting applications

Compared with organic luminescent molecules or inorganic semiconductor quantum dots, CDs have high luminous stability, creating opportunities to replace the aforementioned organic materials or quantum dots. However, their tendency to aggregate by  $\pi$ - $\pi$  stacking between adjacent layers, resulting in PL quenching in the solid-state hinders their widespread application in optoelectronic devices. Such  $\pi$ - $\pi$  stacking causes an increase in uncontrolled electroluminescence due to intermolecular excimer formation, which prevents the formation of pure emission colors in light-emitting devices. Aggregated luminous CDs provide a bright prospect for addressing these problems. Park et al.<sup>[95]</sup> used the functionalization agent to reduce  $\pi$ - $\pi$  stacking between adjacent CDs, thus achieving quenching-resistant PL in the solid-state (Figure 7C). CDs-based white emitting diodes exhibited efficient down-conversion for white light emission with a correlated-color temperature of 5612 K and a high color rendering index of 86.2 at Commission Internationale de l'Éclairage (CIE) coordinate of (0.333, 0.359). In another example,<sup>[34]</sup> the CIE of LED based on the solid-state luminous CDs was (0.285, 0.341). Shao et al.<sup>[30]</sup> synthesized LEDs with various emission colors utilizing self-quenching-resistant solid-state fluorescent CDs. By combining a blue-CDs powder and a self-quenching-resistant solid-state fluorescent CDs powder, a white light LED with the CIE coordinate of (0.31, 0.31) was realized. In the other two examples,<sup>[88, 96]</sup> the carbon nano ring systems were used to prevent aggregation-induced PL quenching and to fabricate high-efficiency LEDs (Figure 7D).

## 5.3. Bioimaging

The bioimaging applications of CDs are severely hampered by aggregation-induced quenching, which result in weak fluorescent images and nonuniform staining. Accordingly, CDs that can stain various kinds of bacteria or cells effectively and real-time without concentration-dependent PL quenching are required. Solid-state fluorescent CDs have been prepared to prevent aggregation-induced quenching through dispersion in solid matrices.<sup>[118-121]</sup> However, many results show that this method has many limitations. Chen et al.<sup>[34]</sup> synthesized a self-quenching-resistant CDs powder utilizing PVA and ethylenediamine, which had a relatively low quantum yield of 35%. Yang et al.<sup>[115]</sup> showed that polyethyleneglycol-functionalized CDs possess weak staining capability (Figure 7E). This is due to the resistance of polyethyleneglycol to protein and reduced interactions between the biological cells and CDs. CDs encapsulated in solid matrices during the synthesis or post-preparation may reduce the bio-affinity interactions between biological cells and CDs and diminish the biocompatibility of the materials. Therefore, aggregation fluorescent CDs without solid matrices are necessary for bioimaging. Zhang et al.<sup>[32]</sup> fabricated self-quenching-resistant solid-state PL CDs without any solid matrices. The multicolor CDs were successfully applied to rapid staining of representative bacterial species, including acid-fast bacteria, gram-positive, and gram-negative. In addition, some pathogenic bacteria could be stained rapidly within 1 min through the smear staining method without any incubation, which is also applicable to the use of liquid incubation methods. Wang et al.<sup>[116]</sup> prepared concentration-dependent fluorescent tunable CDs that can be used as nanoprobe for  $\text{Fe}^{3+}$  detection and multicolor cell imaging (Figure 7F).

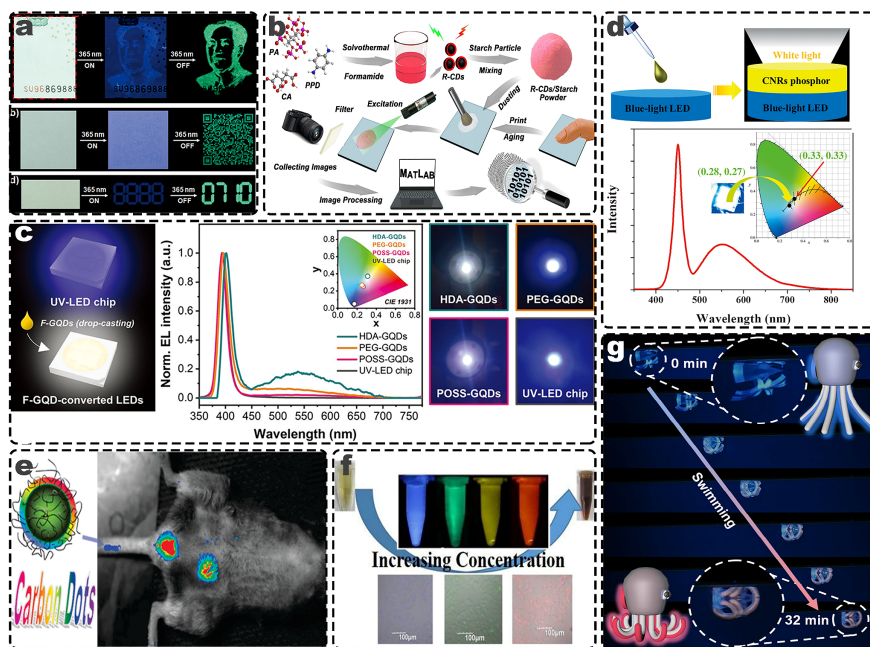


**Figure 7 .** (A) Anti-counterfeiting and information protection applications of the ultralong lifetime room temperature phosphorescence CDs. Reproduced with permission.<sup>[111]</sup> Copyright 2018, Wiley-VCH. (B) Preparation process of CDs/starch powder and its application in latent fingerprints detection. Reproduced with permission.<sup>[114]</sup> Copyright 2020, American Chemical Society. (C) Demonstration of down-converting light-emitting diodes using F-GQDs. Reproduced with permission.<sup>[95]</sup> Copyright 2021, Wiley-VCH. (D) Applications of carbon nanoring phosphors in W-LEDs. Reproduced with permission.<sup>[96]</sup> Copyright 2015, Wiley-VCH. (E) Schematic of CDs used for bioimaging. Reproduced with permission.<sup>[115]</sup> Copyright 2009, American Chemical Society. (F) CDs exhibiting multicolor fluorescence via adjusting their concentrations for biosensing and bioimaging. Reproduced with permission.<sup>[116]</sup> Copyright 2018, Elsevier. (G) The synergistic shape/color change and directional swimming locomotion of the CDs polymer gel-based artificial octopus-like soft robot. Reproduced with permission.<sup>[117]</sup> Copyright 2021, Wiley-VCH.

#### 5.4. Other

The unique properties resulting from the aggregation of CDs are leading to applications in new areas. As shown in figure 7G, Wu et al.<sup>[117]</sup> developed to use special hydrophobic CDs with rotatable surface groups to build the aggregation-induced emission active glycol CDs polymer gel, which could be interfacially bonded to an elastomer to prepare an anisotropic bilayer soft actuator. When the actuator was put in water, glycol will spontaneously diffuse out of the gel layer, leading to a color change from blue dispersive fluorescence to red aggregation-induced emission and shape deformation, whilst the large surface tension gradient promotes voluntary motion. Based on these principles, an artificial soft swimming robot with octopus-shape/color covariation and directional swimming motion was reported.

#### 6. Summary and perspective

As an exciting new type of luminescent carbon-based nanomaterial, CDs received a lot of research attention in the past few years. However, there still many mysteries about the formation process, structure, classification, and luminescence of CDs. Many reports suggest that aggregation plays an important role in CDs, from formation to application, and understanding aggregation processes at different levels it will help resolve many of the mysteries around CDs. In this review, we aimed to highlight the role aggregation in the synthesis of different types of CDs, whilst also highlighting special luminescence properties of CDs that emerge in the aggregate state, including aggregation induced fluorescence quenching and quench-resistant re-

search, aggregation-induced emission, and aggregation-induced room temperature phosphorescence. Finally, the special applications resulting from aggregation of CDs were summarized, including anti-counterfeiting, optoelectronic, bioimaging, and others.

Potential future development directions related to the aggregation of CDs include, but are not limited to, the following

(1) Clarify the structure of CDs. The ambiguity of CDs structure remains a limitation in the field of CDs research. Ideally, bottom-up synthesis methods will be discovered that allow CDs to be fabricated in a rational manner (with accurate size, composition control and structure), thereby allowing better understanding of these variables and aggregation phenomena affect performance. Understanding the precise structure of CDs will help solve many current controversies, including the classification of CDs and luminescence mechanisms, whilst greatly expanding the range of applications.

(2) Shape control adjustment. Shape and size play powerful part in determining the properties of most nanomaterials, but the morphology of the CDs remains difficult to adjust. Some of the above reports have shown that shape adjustment of GQDs and CQDs can be achieved using customized aggregation methods, but much more work is needed in this area. The shape regulation of CPDs remains very difficult. Taking inspiration from the synthesis of inorganic nanoparticles, template and micellar methods are worthwhile strategies to try for morphology-engineering of CDs.

(3) The reasons why some CDs possess aggregation-induced luminescence is unclear, prompting a exact structure description and mechanism analysis. If the mechanism can be properly explained, CDs with particular luminescence phenomena can be more easily customized for more advanced applications.

Despite the above-mentioned challenges, CDs have a bright future. We hope to open this review stimulates wider research linked to understanding aggregation phenomena in CDs.

#### Acknowledgements

This work was supported by the National Natural Science Foundation of China (52122308, 21905253, 51973200, 52103239), the Natural Science Foundation of Henan (202300410372).

#### Conflict of Interests

The authors declare no conflict of interests.

Received: ((will be filled in by the editorial staff)) Revised: ((will be filled in by the editorial staff)) Published online: ((will be filled in by the editorial staff))

#### References

1. N. Hildebrandt, C.M. Spillmann, W.R. Algar, T. Pons, M.H. Stewart, E. Oh, K. Susumu, S.A. Díaz, J.B. Delehanty, I.L. Medintz, *Chem. Rev.* **2017** , 117, 536-711.
2. S.Y. Lim, W. Shen, Z. Gao, *Chem. Soc. Rev.* **2015** , 44, 362-381.
3. K. Sun, Y. Tang, Q. Li, S. Yin, W. Qin, J. Yu, D.T. Chiu, Y. Liu, Z. Yuan, X. Zhang, C. Wu, *ACS Nano* **2016** , 10, 6769-6781.
4. Y. Wu, F. Jelezko, M.B. Plenio, T. Weil, *Angew. Chem., Int. Ed.* **2016** , 55, 6586-6598.
5. L. Shang, S. Dong, G.U. Nienhaus, *Nano Today* **2011** , 6, 401-418.
6. Y. Chen, J.W.Y. Lam, R.T.K. Kwok, B. Liu, B.Z. Tang, *Mater. Horiz.* **2019** , 6, 428-433.
7. Z. Li, X. Ji, H. Xie, B.Z. Tang, *Adv. Mater.* **2021** , 33, 2100021.
8. J. Zhang, B. He, Y. Hu, P. Alam, H. Zhang, J.W.Y. Lam, B.Z. Tang, *Adv. Mater.* **2021** , 33, 2008071.
9. L. Tu, Y. Xie, Z. Li, B. Tang, *SmartMat* **2021** , 2, 326-346.

10. Z. Zhao, H. Zhang, J.W.Y. Lam, B.Z. Tang, *Angew. Chem., Int. Ed.* **2020** , 59, 9888-9907.
11. H. Zhang, Z. Zhao, P.R. McGonigal, R. Ye, S. Liu, J.W.Y. Lam, R.T.K. Kwok, W.Z. Yuan, J. Xie, A.L. Rogach, B.Z. Tang, *Mater. Today* **2020** , 32, 275-292.
12. H. Zhang, X. Zheng, N. Xie, Z. He, J. Liu, N.L.C. Leung, Y. Niu, X. Huang, K.S. Wong, R.T.K. Kwok, H.H.Y. Sung, I.D. Williams, A. Qin, J.W.Y. Lam, B.Z. Tang, *J. Am. Chem. Soc.* **2017** , 139, 16264-16272.
13. X. Xu, R. Ray, Y. Gu, H.J. Ploehn, L. Gearheart, K. Raker, W.A. Scrivens, *J. Am. Chem. Soc.* **2004** , 126, 12736-12737.
14. Y. Ru, S. Lu, *Acta Polym. Sin.* **2022** , 53, 812-827.
15. B. Wang, S. Lu, *Matter* **2022** , 5, 110-149.
16. B. Wang, H. Song, X. Qu, J. Chang, B. Yang, S. Lu, *Coord. Chem. Rev.* **2021** , 442, 214010.
17. W. Meng, X. Bai, B. Wang, Z. Liu, S. Lu, B. Yang, *Energy Environ. Mater.* **2019** , 2, 172-192.
18. Y. Zhai, B. Zhang, R. Shi, S. Zhang, Y. Liu, B. Wang, K. Zhang, G.I.N. Waterhouse, T. Zhang, S. Lu, *Adv. Energy Mater.* **2022** , 12, 2103426.
19. B. Wang, H. Cai, G.I.N. Waterhouse, X. Qu, B. Yang, S. Lu, *Small Sci.* **2022** , 2, 2200012.
20. Y. Ru, L. Ai, T. Jia, X. Liu, S. Lu, Z. Tang, B. Yang, *Nano Today* **2020** , 34, 100953.
21. S. Li, L. Li, H. Tu, H. Zhang, D.S. Silvester, C.E. Banks, G. Zou, H. Hou, X. Ji, *Mater. Today* **2021** , 51, 188-207.
22. L. Ai, Y. Yang, B. Wang, J. Chang, Z. Tang, B. Yang, S. Lu, *Sci. Bull.* **2021** , 66, 839-856.
23. S. Zhu, Y. Song, X. Zhao, J. Shao, J. Zhang, B. Yang, *Nano Res.* **2015** , 8, 355-381.
24. J. Shen, Y. Zhu, X. Yang, C. Li, *Chem. Commun.* **2012** , 48, 3686-3699.
25. M.E. Khan, A. Mohammad, T. Yoon, *Chemosphere* **2022** , 302, 134815.
26. S. Tao, T. Feng, C. Zheng, S. Zhu, B. Yang, *J. Phys. Chem. Lett.* **2019** , 10, 5182-5188.
27. S.N. Baker, G.A. Baker, *Angew. Chem., Int. Ed.* **2010** , 49, 6726-6744.
28. C. Kang, S. Tao, F. Yang, B. Yang, *Aggregate* **2022** , 3, e169.
29. Y. Li, H. Lin, C. Luo, Y. Wang, C. Jiang, R. Qi, R. Huang, J. Travas-sejdic, H. Peng, *RSC Adv.* **2017** , 7, 32225-32228.
30. J. Shao, S. Zhu, H. Liu, Y. Song, S. Tao, B. Yang, *Adv. Sci.* **2017** , 4, 1700395.
31. Y. Su, Z. Xie, M. Zheng, *J. Colloid Interface Sci.* **2020** , 573, 241-249.
32. Y. Zhang, C. Li, Y. Fan, C. Wang, R. Yang, X. Liu, L. Zhou, *Nanoscale* **2016** , 8, 19744-19753.
33. B.E. Kwak, H.J. Yoo, D.H. Kim, *Adv. Opt. Mater.* **2019** , 7, 1900932.
34. Y. Chen, M. Zheng, Y. Xiao, H. Dong, H. Zhang, J. Zhuang, H. Hu, B. Lei, Y. Liu, *Adv. Mater.* **2016** , 28, 312-318.
35. L.A. Ponomarenko, F. Schedin, M.I. Katsnelson, R. Yang, E.W. Hill, K.S. Novoselov, A.K. Geim, *Science* **2008** , 320, 356-358.
36. Z. Jin, P. Owour, S. Lei, L. Ge, *Curr. Opin. Colloid Interface Sci.* **2015** , 20, 439-453.
37. G. Eda, Y.-Y. Lin, C. Mattevi, H. Yamaguchi, H.-A. Chen, I.-S. Chen, C.-W. Chen, M. Chhowalla, *Adv. Mater.* **2010** , 22, 505-509.

38. M.A. Sk, A. Ananthanarayanan, L. Huang, K.H. Lim, P. Chen, J. Mater. Chem. C **2014** , 2, 6954-6960.
39. S.H. Jin, D.H. Kim, G.H. Jun, S.H. Hong, S. Jeon, ACS Nano**2013** , 7, 1239-1245.
40. Y. Yan, J. Gong, J. Chen, Z. Zeng, W. Huang, K. Pu, J. Liu, P. Chen, Adv. Mater. **2019** , 31, 1808283.
41. H. Yoon, M. Park, J. Kim, T.G. Novak, S. Lee, S. Jeon, Chem. Phys. Rev. **2021** , 2, 031303.
42. C. Xia, S. Zhu, T. Feng, M. Yang, B. Yang, Adv. Sci. **2019** , 6, 1901316.
43. Z. Luo, G. Qi, K. Chen, M. Zou, L. Yuwen, X. Zhang, W. Huang, L. Wang, Adv. Funct. Mater. **2016** , 26, 2739-2744.
44. H. Yoon, Y.H. Chang, S.H. Song, E.-S. Lee, S.H. Jin, C. Park, J. Lee, B.H. Kim, H.J. Kang, Y.-H. Kim, S. Jeon, Adv. Mater. **2016** , 28, 5255-5261.
45. J. Ali, G.-u.-d. Siddiqui, Y.J. Yang, K.T. Lee, K. Um, K.H. Choi, RSC Adv. **2016** , 6, 5068-5078.
46. Z. Zhang, J. Zhang, N. Chen, L. Qu, Energy Environ. Sci.**2012** , 5, 8869-8890.
47. L. Li, G. Wu, G. Yang, J. Peng, J. Zhao, J.-J. Zhu, Nanoscale**2013** , 5, 4015-4039.
48. H. Jin, H. Huang, Y. He, X. Feng, S. Wang, L. Dai, J. Wang, J. Am. Chem. Soc. **2015** , 137, 7588-7591.
49. R. Liu, D. Wu, X. Feng, K. Müllen, J. Am. Chem. Soc. **2011** , 133, 15221-15223.
50. L. Wang, Y. Wang, T. Xu, H. Liao, C. Yao, Y. Liu, Z. Li, Z. Chen, D. Pan, L. Sun, M. Wu, Nat. Commun. **2014** , 5, 5357.
51. Y. Dong, J. Shao, C. Chen, H. Li, R. Wang, Y. Chi, X. Lin, G. Chen, Carbon **2012** , 50, 4738-4743.
52. S.H. Lee, D.Y. Kim, J. Lee, S.B. Lee, H. Han, Y.Y. Kim, S.C. Mun, S.H. Im, T.-H. Kim, O.O. Park, Nano Lett. **2019** , 19, 5437-5442.
53. L.-s. Li, X. Yan, J. Phys. Chem. Lett. **2010** , 1, 2572-2576.
54. X. Yan, X. Cui, L.-s. Li, J. Am. Chem. Soc. **2010** , 132, 5944-5945.
55. T.-F. Yeh, W.-L. Huang, C.-J. Chung, I.T. Chiang, L.-C. Chen, H.-Y. Chang, W.-C. Su, C. Cheng, S.-J. Chen, H. Teng, J. Phys. Chem. Lett.**2016** , 7, 2087-2092.
56. Y. Dong, C. Chen, X. Zheng, L. Gao, Z. Cui, H. Yang, C. Guo, Y. Chi, C.M. Li, J. Mater. Chem. **2012** , 22, 8764-8766.
57. Y. Yan, J. Chen, N. Li, J. Tian, K. Li, J. Jiang, J. Liu, Q. Tian, P. Chen, ACS Nano **2018** , 12, 3523-3532.
58. Y.-P. Sun, B. Zhou, Y. Lin, W. Wang, K.A.S. Fernando, P. Pathak, M.J. Meziani, B.A. Harruff, X. Wang, H. Wang, P.G. Luo, H. Yang, M.E. Kose, B. Chen, L.M. Veca, S.-Y. Xie, J. Am. Chem. Soc. **2006** , 128, 7756-7757.
59. H. Tao, K. Yang, Z. Ma, J. Wan, Y. Zhang, Z. Kang, Z. Liu, Small**2012** , 8, 281-290.
60. S. Hu, J. Liu, J. Yang, Y. Wang, S. Cao, J. Nanopart. Res.**2011** , 13, 7247-7252.
61. L. Tang, R. Ji, X. Cao, J. Lin, H. Jiang, X. Li, K.S. Teng, C.M. Luk, S. Zeng, J. Hao, S.P. Lau, ACS Nano **2012** , 6, 5102-5110.
62. C.-B. Ma, Z.-T. Zhu, H.-X. Wang, X. Huang, X. Zhang, X. Qi, H.-L. Zhang, Y. Zhu, X. Deng, Y. Peng, Y. Han, H. Zhang, Nanoscale**2015** , 7, 10162-10169.
63. J. Xu, S. Sahu, L. Cao, P. Anilkumar, K.N. Tackett II, H. Qian, C.E. Bunker, E.A. Guliants, A. Parenzan, Y.-P. Sun, ChemPhysChem**2011** , 12, 3604-3608.
64. L. Cao, M.J. Meziani, S. Sahu, Y.-P. Sun, Acc. Chem. Res.**2013** , 46, 171-180.

65. L. Wang, S.-J. Zhu, H.-Y. Wang, S.-N. Qu, Y.-L. Zhang, J.-H. Zhang, Q.-D. Chen, H.-L. Xu, W. Han, B. Yang, H.-B. Sun, *ACS Nano* **2014** , 8, 2541-2547.
66. J. Liu, D. Li, K. Zhang, M. Yang, H. Sun, B. Yang, *Small* **2018** , 14, 1703919.
67. Y. Song, S. Zhu, J. Shao, B. Yang, *J. Polym. Sci., Part A: Polym. Chem.* **2017** , 55, 610-615.
68. S. Tao, S. Zhu, T. Feng, C. Xia, Y. Song, B. Yang, *Mater. Today Chem.* **2017** , 6, 13-25.
69. S. Zhu, Q. Meng, L. Wang, J. Zhang, Y. Song, H. Jin, K. Zhang, H. Sun, H. Wang, B. Yang, *Angew. Chem., Int. Ed.* **2013** , 52, 3953-3957.
70. S. Tao, Y. Song, S. Zhu, J. Shao, B. Yang, *Polymer* **2017** , 116, 472-478.
71. S. Tao, S. Zhu, T. Feng, C. Zheng, B. Yang, *Angew. Chem., Int. Ed.* **2020** , 59, 9826-9840.
72. X. Wang, L. Cao, S.-T. Yang, F. Lu, M.J. Meziani, L. Tian, K.W. Sun, M.A. Bloodgood, Y.-P. Sun, *Angew. Chem., Int. Ed.* **2010** , 49, 5310-5314.
73. W. Kwon, S. Do, J.-H. Kim, M. Seok Jeong, S.-W. Rhee, *Sci. Rep.* **2015** , 5, 12604.
74. M. Shamsipur, A. Barati, A.A. Taherpour, M. Jamshidi, *J. Phys. Chem. Lett.* **2018** , 9, 4189-4198.
75. Y. Song, S. Zhu, S. Zhang, Y. Fu, L. Wang, X. Zhao, B. Yang, *J. Mater. Chem. C* **2015** , 3, 5976-5984.
76. H. Ding, J.-S. Wei, P. Zhang, Z.-Y. Zhou, Q.-Y. Gao, H.-M. Xiong, *Small* **2018** , 14, 1800612.
77. S. Zhu, J. Zhang, L. Wang, Y. Song, G. Zhang, H. Wang, B. Yang, *Chem. Commun.* **2012** , 48, 10889-10891.
78. J. Gu, W. Wang, Q. Zhang, Z. Meng, X. Jia, K. Xi, *RSC Adv.* **2013** , 3, 15589-15591.
79. X. Yang, L. Ai, J. Yu, G.I.N. Waterhouse, L. Sui, J. Ding, B. Zhang, X. Yong, S. Lu, *Sci. Bull.* **2022** , 67, 1450-1457.
80. B. Wang, Z. Wei, L. Sui, J. Yu, B. Zhang, X. Wang, S. Feng, H. Song, X. Yong, Y. Tian, B. Yang, S. Lu, *Light: Sci. Appl.* **2022** , 11, 172.
81. C. Xia, S. Tao, S. Zhu, Y. Song, T. Feng, Q. Zeng, J. Liu, B. Yang, *Chem. - Eur. J.* **2018** , 24, 11303-11308.
82. J. Yang, L. Guo, X. Yong, T. Zhang, B. Wang, H. Song, Y.S. Zhao, H. Hou, B. Yang, J. Ding, S. Lu, *Angew. Chem., Int. Ed.* **2022** , 134, e202207817.
83. A.K. Pearce, T.R. Wilks, M.C. Arno, R.K. O'Reilly, *Nat. Rev. Chem.* **2021** , 5, 21-45.
84. M. Chen, B. Wu, J. Yang, N. Zheng, *Adv. Mater.* **2012** , 24, 862-879.
85. Y. Chen, Z. Fan, Z. Zhang, W. Niu, C. Li, N. Yang, B. Chen, H. Zhang, *Chem. Rev.* **2018** , 118, 6409-6455.
86. F. Yuan, T. Yuan, L. Sui, Z. Wang, Z. Xi, Y. Li, X. Li, L. Fan, Z.a. Tan, A. Chen, M. Jin, S. Yang, *Nat. Commun.* **2018** , 9, 2249.
87. S. Subedi, A.K. Rella, L.G. Trung, V. Kumar, S.-W. Kang, *ACS Nano* **2022** , 16, 6480-6492.
88. T. Meng, Z. Wang, T. Yuan, X. Li, Y. Li, Y. Zhang, L. Fan, *Angew. Chem., Int. Ed.* **2021** , 60, 16343-16348.
89. Y. Xiong, X. Zhang, A.F. Richter, Y. Li, A. Döring, P. Kasák, A. Popelka, J. Schneider, S.V. Kershaw, S.J. Yoo, J.-G. Kim, W. Zhang, W. Zheng, E.V. Ushakova, J. Feldmann, A.L. Rogach, *ACS Nano* **2019** , 13, 12024-12031.
90. Q. Li, B. Chen, B. Xing, *Environ. Sci. Technol.* **2017** , 51, 1364-1376.

91. X.-X. Ba, L. Zhang, Y.-L. Yin, F.-L. Jiang, P. Jiang, Y. Liu, J. Colloid Interface Sci. **2020** , 565, 77-85.
92. H. Zhang, Z. Zhao, A.T. Turley, L. Wang, P.R. McGonigal, Y. Tu, Y. Li, Z. Wang, R.T.K. Kwok, J.W.Y. Lam, B.Z. Tang, Adv. Mater.**2020** , 32, 2001457.
93. L. Chen, S. Xu, D. McBranch, D. Whitten, J. Am. Chem. Soc.**2000** , 122, 9302-9303.
94. S. Han, X. Chen, Y. Hu, L. Han, Dyes Pigm. **2021** , 187, 109090.
95. M. Park, Y. Jeong, H.S. Kim, W. Lee, S.-H. Nam, S. Lee, H. Yoon, J. Kim, S. Yoo, S. Jeon, Adv. Funct. Mater. **2021** , 31, 2102741.
96. X. Li, Y. Liu, X. Song, H. Wang, H. Gu, H. Zeng, Angew. Chem., Int. Ed. **2015** , 54, 1759-1764.
97. J. Ren, L. Stagi, P. Innocenzi, Prog. Solid State Chem.**2021** , 62, 100295.
98. M. Park, H. Yoon, J. Lee, J. Kim, J. Lee, S.-E. Lee, S. Yoo, S. Jeon, Adv. Mater. **2018** , 30, 1802951.
99. D. Zhou, D. Li, P. Jing, Y. Zhai, D. Shen, S. Qu, A.L. Rogach, Chem. Mater. **2017** , 29, 1779-1787.
100. J. Luo, Z. Xie, J.W.Y. Lam, L. Cheng, H. Chen, C. Qiu, H.S. Kwok, X. Zhan, Y. Liu, D. Zhu, B.Z. Tang, Chem. Commun. **2001** , 1740-1741.
101. Z.X. Liu, Z.L. Wu, M.X. Gao, H. Liu, C.Z. Huang, Chem. Commun.**2016** , 52, 2063-2066.
102. H. Yang, Y. Liu, Z. Guo, B. Lei, J. Zhuang, X. Zhang, Z. Liu, C. Hu, Nat. Commun. **2019** , 10, 1789.
103. S. Chen, J.-W. Liu, M.-L. Chen, X.-W. Chen, J.-H. Wang, Chem. Commun. **2012** , 48, 7637-7639.
104. X. Li, S. Zhu, B. Xu, K. Ma, J. Zhang, B. Yang, W. Tian, Nanoscale**2013** , 5, 7776-7779.
105. K. Jiang, X. Gao, X. Feng, Y. Wang, Z. Li, H. Lin, Angew. Chem., Int. Ed. **2020** , 59, 1263-1269.
106. S. Tao, S. Lu, Y. Geng, S. Zhu, S.A.T. Redfern, Y. Song, T. Feng, W. Xu, B. Yang, Angew. Chem., Int. Ed. **2018** , 57, 2393-2398.
107. B. Wang, Z. Sun, J. Yu, G.I.N. Waterhouse, S. Lu, B. Yang, SmartMat**2022** , 3, 337-348.
108. M.-M. Fang, J. Yang, Z. Li, Chin. J. Polym. Sci. **2019** , 37, 383-393.
109. N. Gan, H. Shi, Z. An, W. Huang, Adv. Funct. Mater. **2018** , 28, 1802657.
110. K. Jiang, Y. Wang, Z. Li, H. Lin, Mater. Chem. Front.**2020** , 4, 386-399.
111. K. Jiang, Y. Wang, X. Gao, C. Cai, H. Lin, Angew. Chem., Int. Ed.**2018** , 57, 6216-6220.
112. J. Tan, Q. Li, S. Meng, Y. Li, J. Yang, Y. Ye, Z. Tang, S. Qu, X. Ren, Adv. Mater. **2021** , 33, 2006781.
113. J. Chen, J.-S. Wei, P. Zhang, X.-Q. Niu, W. Zhao, Z.-Y. Zhu, H. Ding, H.-M. Xiong, ACS Appl. Mater. Interfaces **2017** , 9, 18429-18433.
114. X.-Y. Dong, X.-Q. Niu, Z.-Y. Zhang, J.-S. Wei, H.-M. Xiong, ACS Appl. Mater. Interfaces **2020** , 12, 29549-29555.
115. S.-T. Yang, L. Cao, P.G. Luo, F. Lu, X. Wang, H. Wang, M.J. Meziani, Y. Liu, G. Qi, Y.-P. Sun, J. Am. Chem. Soc. **2009** , 131, 11308-11309.
116. C. Wang, T. Hu, Z. Wen, J. Zhou, X. Wang, Q. Wu, C. Wang, J. Colloid Interface Sci. **2018** , 521, 33-41.
117. S. Wu, H. Shi, W. Lu, S. Wei, H. Shang, H. Liu, M. Si, X. Le, G. Yin, P. Theato, T. Chen, Angew. Chem., Int. Ed. **2021** , 60, 21890-21898.
118. X. Li, S. Zhang, S.A. Kulinich, Y. Liu, H. Zeng, Sci. Rep.**2014** , 4, 4976.

119. Y. Deng, D. Zhao, X. Chen, F. Wang, H. Song, D. Shen, *Chem. Commun.* **2013** , 49, 5751-5753.
120. Y. Deng, X. Chen, F. Wang, X. Zhang, D. Zhao, D. Shen, *Nanoscale* **2014** , 6, 10388-10393.
121. F. Wang, Z. Xie, H. Zhang, C.-y. Liu, Y.-g. Zhang, *Adv. Funct. Mater.* **2011** , 21, 1027-1031.



Yi Ru is currently a Ph.D. student of College of Chemistry under the supervision of Prof. Siyu Lu at Zhengzhou University. Her major research focuses on carbon dots and perovskite.



Siyu Lu is a professor of the College of Chemistry, Zhengzhou University. He received his Ph.D. degree in polymer physics and chemistry under the supervision of Prof. Bai Yang at Jilin University. His research interests relate to the design, preparation, properties of photoelectric nanocrystals (carbon dots, semiconductors, etc.) and their applications in catalysis and fluorescence.

Contents:

Carbon dots (CDs) has excellent photoluminescence properties. Aggregation plays an important role in both the formation of CDs and their fluorescence, yet is seldom studied in detail. This review aims to fill this knowledge gap. We first discuss how aggregation leads to the formation of different types of CDs, and the impact on morphology, luminescence and applications.

**Keyword** carbon dots, aggregation, special morphology, special luminescence, special application

Yi Ru, Geoffrey I. N. Waterhouse, Siyu Lu\*

Title: Aggregation in carbon dots

ToC figure



